HHS Public Access

Author manuscript

Neuroimage. Author manuscript; available in PMC 2018 February 01.

Published in final edited form as:

Neuroimage. 2017 February 01; 146: 715–723. doi:10.1016/j.neuroimage.2016.09.063.

Multiparametric imaging of brain hemodynamics and function using gas-inhalation MRI

Peiying Liu[a], **Babu G. Welch**[b,c], **Yang Li**[a,d], **Hong Gu**[e], **Darlene King**[b], **Yihong Yang**[e], **Marco Pinho**[c], and **Hanzhang Lu**[a,*]

[a]Department of Radiology, Johns Hopkins University School of Medicine, Baltimore, MD 21287

[b]Department of Neurological Surgery, UT Southwestern Medical Center, Dallas, TX 75390

[c]Department of Radiology, UT Southwestern Medical Center, Dallas, TX 75390

[d]Biomedical Engineering Graduate Program, UT Southwestern Medical Center, Dallas, TX 75390

[e]Neuroimaging Research Branch, National Institute on Drug Abuse, National Institutes of Health, Baltimore, Maryland 21224

Abstract

Diagnosis and treatment monitoring of cerebrovascular diseases routinely require hemodynamic imaging of the brain. Current methods either only provide part of the desired information or require the injection of multiple exogenous agents. In this study, we developed a multiparametric imaging scheme for the imaging of brain hemodynamics and function using gas-inhalation MRI. The proposed technique uses a single MRI scan to provide simultaneous measurements of baseline venous cerebral blood volume (vCBV), cerebrovascular reactivity (CVR), bolus arrival time (BAT), and resting-state functional connectivity (fcMRI). This was achieved with a novel, concomitant O_2 and CO_2 gas inhalation paradigm, rapid MRI image acquisition with a 9.3 min BOLD sequence, and an advanced algorithm to extract multiple hemodynamic information from the same dataset. In healthy subjects, CVR and vCBV values were 0.23±0.03 %/mmHg and 0.0056±0.0006 %/mmHg, respectively, with a strong correlation (r=0.96 for CVR and r=0.91 for vCBV) with more conventional, separate acquisitions that take twice the scan time. In patients with Moyamoya syndrome, CVR in the stenosis-affected flow territories (typically anterior-cerebral-artery, ACA, and middle-cerebral-artery, MCA, territories) was significantly lower than that in posterior-cerebral-artery (PCA), which typically has minimal stenosis, flow territories (0.12±0.06 %/mmHg vs. 0.21±0.05 %/mmHg, p<0.001). BAT of the gas bolus was significantly longer (p=0.008) in ACA/MCA territories, compared to PCA, and the maps were consistent with the conventional contrast-enhanced CT perfusion method. FcMRI networks were robustly identified from the gas-inhalation MRI data after factoring out the influence of CO_2 and O_2 on the

*Corresponding author: Hanzhang Lu, Ph.D., Department of Radiology, Johns Hopkins University School of Medicine, 600 N. Wolfe Street, Park 322, Baltimore, MD 21287, hanzhang.lu@jhu.edu, Phone: 410-955-1431, Fax: 410-614-1977.

Conflicts of interest

The authors have no conflicts of interest or financial disclosures to report.

signal time course. The spatial correspondence between the gas-data-derived fcMRI maps and those using a separate, conventional fcMRI scan was excellent, showing a spatial correlation of 0.58±0.17 and 0.64±0.20 for default mode network and primary visual network, respectively. These findings suggest that advanced gas-inhalation MRI provides reliable measurements of multiple hemodynamic parameters within a clinically acceptable imaging time and is suitable for patient examinations.

Keywords

Cerebrovascular reactivity; venous cerebral blood volume; bolus arrival time; resting-state functional connectivity; hypercapnia; hyperoxia

1. Introduction

Medical imaging has provided a wealth of tools to evaluate the brain's vascular function. It plays an important role in the management of various cerebrovascular diseases and conditions, including arterial stenosis (Donahue et al., 2013; Gupta et al., 2012; Mandell et al., 2008; Mikulis et al., 2005), stroke (Geranmayeh et al., 2015), small vessel disease (Greenberg, 2006), brain tumors (Lu et al., 2008), traumatic brain injury (Chan et al., 2015), and substance abuse (Han et al., 2008).

In current clinical practice, Computed Tomography Perfusion (CTP) and magnetic resonance imaging (MRI) with gadolinium-based dynamic susceptibility contrast (DSC) are often used to examine baseline vascular properties such as cerebral blood flow (CBF) (Detre et al., 1992; Wintermark et al., 2000), cerebral blood volume (CBV) (Ostergaard et al., 1996) and arterial arrival delay (Lv et al., 2013; Reichenbach et al., 1999). In situations where baseline measurements are found to be insufficient to make treatment decisions, a “stress-test” of brain vasculature is usually required to collect cerebrovascular reactivity information (Burt et al., 1992; Chollet et al., 1989; Pillai and Zaca, 2011). This requires a separate visit during which a vasoactive challenge, e.g. injection of acetazolamide, is applied and vascular reactivity is assessed using radionuclide methods such as Single-Photon-Emission-Computer-Tomography (SPECT) or Positron Emission Tomography (PET) (Hirano et al., 1994; Ogasawara et al., 2003). Additionally, resting-state functional MRI is being increasingly used in patients with cerebrovascular diseases to evaluate their brain function (Carter et al., 2012; Park et al., 2011), which requires another imaging exam in the patient's workup schedule.

A major limitation of the current clinical practice is that collection of all information described above requires separate exams and, sometimes, separate visits. This limitation increases patient burden and significantly escalates the cost of care. Moreover, PCT, SPECT and PET scans involve the exposure to ionizing radiation (Hirano et al., 1994; Ogasawara et al., 2003; Reichenbach et al., 1999; Wintermark et al., 2000). MRI based perfusion studies do not require ionizing radiation; however, the most commonly used MR contrast agent, gadolinium-based chelate, cannot be applied to patients with poor renal function, due to risk of development of nephrogenic systemic fibrosis (NSF) (Marckmann et al., 2006). Even for patients with healthy renal function, residuals of the injected gadolinium-based contrast

agent (GBCA) can apparently cross the blood-brain-barrier and deposit in the brain (McDonald et al., 2015). While no clinical symptoms have been characterized, it nonetheless presents a safety concern when used repeatedly (http://www.fda.gov/Drugs/DrugSafety/ucm455386.htm). Due to the concerns of radiation safety and dose-restrictions, these methods are generally not used for disease surveillance and treatment monitoring. In all, current clinical practice of hemodynamic imaging of the brain could be improved in terms of efficiency, cost, and risk management.

Therefore, we aim to develop an MRI procedure to provide a one-stop-shop imaging of baseline CBV, cerebrovascular reactivity (CVR), bolus arrival time (BAT), and functional connectivity (FC) in one exam, with no exogenous contrast agent. The technique is based on concomitant modulation of CO_2 and O_2 content in inspired gas while collecting blood-oxygenation-level-dependent (BOLD) MRI images. Both CO_2 and O_2 are endogenous to the body, thus modulation within the typical physiological range is safe (Brueckl et al., 2006; Donahue et al., 2014; Spano et al., 2013). CO_2 is a potent vasodilator (Brian, 1998) and can cause perfusion (thereby BOLD MRI signal) changes in healthy vasculature (Bright et al., 2011; Donahue et al., 2013; Han et al., 2008; Lu et al., 2011; Mandell et al., 2008; Marshall et al., 2014; Mikulis et al., 2005; Sheng et al., 2015; Yezhuvath et al., 2012). Short-duration O_2 inhalation does not cause vasodilation or vasoconstriction (Mark and Pike, 2012; Xu et al., 2012), but it can serve as an intravascular contrast agent and alters BOLD MRI signal via its effect on the concentration of deoxyhemoglobin. Thus, MRI signal changes associated with O_2 inhalation provides an estimation of baseline venous cerebral blood volume (vCBV) (Blockley et al., 2013; Bulte et al., 2007). In our technique, the timing of CO_2 and O_2 modulation was designed such that their contributions to BOLD signal could be separately assessed. Outputs of the technique include CVR, vCBV, BAT, and FC. CVR is obtained from BOLD response to arterial CO_2 change. Baseline vCBV is obtained from BOLD response to arterial O_2 change. BAT is obtained from the voxel-wise delay between the physiological (i.e. end-tidal CO_2 and O_2 measured from the exhaled air) and MRI signals. FC is obtained from the residual BOLD signal after factoring out the CO_2 and O_2 modulation effects.

In the present study, we provide the first evidence of the proposed multiparametric imaging technique in a group of healthy volunteers. We further demonstrate the clinical utility of the technique in detecting hemodynamic deficits in patients with Moyamoya syndrome, which is a cerebrovascular disease characterized by non-atherosclerotic intracranial stenosis. We compared the concomitant CVR and vCBV measurements to the results of separate CO_2 and O_2 modulation sessions. The BAT measurement was validated by comparison with similar measurements obtained by the current standard, CT Perfusion (CTP). FC maps obtained with our technique were compared with conventional resting-state fMRI scans. We hypothesized that the hemodynamic maps obtained from our method is comparable to those obtained from conventional methods.

2. Materials and methods

2.1 Participants

A total of sixteen human participants were studied, seven of which were healthy volunteers (4 males, age 29.4±5.4 years, range 22-36 years) and nine of which were patients with clinical diagnosis of Moyamoya syndrome. The subjects had no contraindications to MRI scanning (e.g., pacemaker, implanted metallic objects, claustrophobia). Each of the Moyamoya patients received a CT perfusion scan as part of their clinical workup, which allowed the validation of the new method with an existing technique. Each subject gave informed written consent before participating in the study. The study protocol was approved by the Institutional Review Board of the University of Texas Southwestern Medical Center.

2.2 MRI Experiment

All MR imaging experiments were conducted on a 3 Tesla MR system using a 32-channel receive-only head coil (Philips Medical Systems, Best, The Netherlands). The body coil was used for RF transmission. For healthy volunteers, each subject underwent a "concomitant CO_2 and O_2" breathing task (Figure 1, detailed in a later section). For comparison, these subjects also received a "CO_2-only" breathing task and an "O_2-only" breathing task. The order of the concomitant and single-gas challenges was randomized and counterbalanced across subjects. BOLD images were continuously acquired throughout the period when the subject performed the breathing task, with the following parameters: FOV = 220×220×90 mm^3, voxel size = 3.4×3.4×5mm^3, TR/TE=800/22.5ms, 18 slices, 701 dynamics, and scan duration 9 minutes and 20 seconds. Note that these TR and TE values were optimized such that there is no artifactual negative CVR due to blood volume effects (Ravi et al., 2015).

For the study in Moyamoya patients, each subject also received the concomitant CO_2 and O_2 breathing task. To validate the functional connectivity results obtained from the breathing data, a conventional resting-state fMRI scan was performed, during which the subject was instructed to keep their eyes open and fixate on a white crosshair at the center of a black screen. The imaging parameters for both the breathing task and the resting-state scan were: BOLD sequence, FOV = 205×205×151 mm^3, TR/TE=1510/21ms, 3.2mm isotropic voxels, whole brain coverage using 36 slices with 1mm gap, 372 dynamics, and scan duration 9 minutes and 20 seconds. Additionally, a standard time-of-flight intracranial MR angiogram was performed to evaluate vessel stenosis and a T2-weighted Fluid-attenuated-inversion-recovery (FLAIR) sequence was performed to identify brain parenchymal injury.

For all participants, a T_1-weighted high-resolution image was acquired for anatomic reference. The scan used a Magnetization-Prepared-Rapid-Acquisition-of-Gradient-Echo (MPRAGE) sequence with the following imaging parameters: 3D, TR = 2100ms, TI = 1100ms, FOV = 256×256×160 mm^3, sagittal slices, voxel size=1×1×1mm^3, scan duration = 4 min.

2.3 Delivery of special gas mixture inside an MRI scanner

The MRI-compatible gas delivery system has been described previously (Lu et al., 2014; Yezhuvath et al., 2009). Briefly, prior to the breathing task, the subject was fitted with a nose

clip, so that they can breathe room air and prepared gases through a mouthpiece (Figure 1b). The prepared gases were contained in Douglas bags and delivered through a two-way non-rebreathing valve and mouthpiece combination (Hans Rudolph, 2600 series, Shawnee, KS). A research assistant was inside the magnet room throughout the experiment to switch a valve that controls the source of the inspired air, as well as monitoring the subject. End-tidal CO_2 ($EtCO_2$), CO_2 concentration in the lung and thus approximating arterial CO_2 levels, was recorded throughout the breathing task using a capnograph device (Capnogard, Model 1265, Novametrix Medical Systems, CT). EtO_2 was recorded using an O_2 monitoring device (Biopac O2100c, BIOPAC Systems, Inc., Goleta, CA). Heart rate and arterial oxygen saturation were monitored using a pulse oximeter (Invivo Expression, Invivo Corporation, Gainesville, FL).

2.4 Gas composition and time paradigm of the single-gas and concomitant breathing tasks

The concomitant paradigm is based on the separate CO_2 and O_2 paradigm. Figure S1a shows the breathing paradigm for CO_2-only task. The subject breathes room-air (0.03% CO_2, 21% O_2) and a gas mixture of 5% CO_2, 21% O_2, and 74% N_2 in an interleaved fashion. For O_2-only breathing task (Figure S1b), the subject breathes room-air and a gas mixture of 0% CO_2, 95% O_2, and 5% N_2 in an interleaved fashion. Figure S1c shows the "concomitant CO_2 and O_2" breathing task. One can see that, in this paradigm, there is a state under which hypercapnia and hyperoxia are induced at the same time (yellow block in Figure S1c). This is NOT simply mixing the above-referenced CO_2 (blue block) and O_2 (red block) gases together. Instead, the proper approach is to maintain the CO_2 content in the gas identical to the CO_2-only challenge and maintain the O_2-content identical to the O_2-only challenge, by reducing N_2 content. Specifically, the simultaneous hypercapnia/hyperoxia state is achieved by using a new gas mixture containing 5% CO_2, 95% O_2, and 0% N_2. This also explains why we did not use 100% O_2 for the hyperoxia-only challenge. Should we have used 100% O_2, the simultaneous challenge would have to use 5% CO_2 and 100% O_2, which is mathematically not possible.

The exact timing in terms of block durations is also depicted in Figure S1c.

2.5 Estimation of multiple hemodynamic maps from the concomitant CO_2 and O_2 data

Data analysis of the concomitant CO_2 and O_2 data was conducted using the software Statistical Parametric Mapping (SPM, University College London, UK) and in-house MATLAB (MathWorks, Natick, MA) scripts. In pre-processing, motion correction was performed by realigning the image volumes of the BOLD MRI images to the first volume within the time series. The BOLD images were then normalized to the image template of Montreal Neurological Institute (MNI) via T_1-weighted high-resolution anatomic image and were resampled to a voxel size of $2\times2\times2$ mm^3. As the final step of the pre-processing, all BOLD image volumes were smoothed using a Gaussian filter with a full-width-half-maximum (FWHM) of 8mm.

The post-processing followed the steps outlined in Figure 2. *Step 1:* estimation of bolus arrival time (BAT). BAT of the inhaled gas was quantified as the time delay between the end-tidal time courses (which has been corrected for sampling tubing delay) and the BOLD

signal time courses. We have tested several approaches for this calculation and propose the following procedure for best performance. We used BOLD time course in a reference brain region as an intermediate and calculate voxel-by-voxel delay time between each brain voxels and the reference time course. For healthy volunteers, the reference region was chosen to be whole brain gray matter. For Moyamoya patients, since anterior and middle cerebral arteries could be affected but posterior cerebral circulation is thought to be intact in this disease, cerebellum gray matter time course was used as the reference. The best delay was determined by shifting the reference time course from −10·TR to +80·TR at an interval of TR and, at each shift step, performing linear regression between the voxel time course and the shifted reference. The shift that corresponds to the least residual signal in the regression analysis will be used as the best delay. Next, the delay between the reference time course and the end-tidal time course were calculated in a similar fashion. This was performed separately for $EtCO_2$ and EtO_2 time courses. The voxel-by-voxel BAT was then obtained by the sum of the voxel-vs-reference delay and the reference-vs-end-tidal time course delay. One therefore obtains a CO_2 BAT and an O_2 BAT map, although their image contrast is the same.

Step 2: estimation of CVR and vCBV (Figure 2). After obtaining the BAT maps, the $EtCO_2$ and EtO_2 time courses were shifted for each voxel. Then voxel-wise regression was performed, with the BOLD time course of each voxel as dependent variable and the BAT-shifted end-tidal time courses as independent variable. The magnitudes of CVR and vCBV of each voxel were calculated using the coefficients of the linear regression (Thomas et al., 2014; Yezhuvath et al., 2009), i.e., $CVR(i, j, k) = b(i, j, k)/[c(i, j, k) + \min(EtCO_2) \cdot b(i, j, k)]$ and $vCBV(i, j, k) = a(i, j, k)/[c(i, j, k) + \min(EtO_2) \cdot a(i, j, k)]$, and is written in %ΔBOLD signal per mmHg CO_2 and %ΔBOLD signal per mmHg O_2, respectively.

Step 3: estimation of functional connectivity maps (Figure 2). For functional connectivity analysis, the residual BOLD time course after factoring out the CO_2 and O_2 influences, i.e., $\Delta BOLD/BOLD_0 - a \cdot EtO_2 - b \cdot EtCO_2$, was first calculated on a voxel-by-voxel basis, which forms a new 4D dataset. Then the residual 4D data were detrended and bandpass-filtered to 0.01–0.1 Hz to retain the low-frequency fluctuation components, which represent the main signal for functional connectivity. Next, independent component analysis (ICA) was performed using MELODIC (FMRIB Analysis Group, Oxford University). Group ICA analysis was used for the healthy volunteers, and individual ICA analysis was performed for Moyamoya patients. The component number of the ICA analysis was set to be 20, following previous literature (Lerman et al., 2014). The brain networks were identified by evaluating the similarity in the spatial extent between the ICA components and previously published results (Beckmann et al., 2005) using spatial cross-correlation. Visual inspection was performed to verify the identified networks.

3. Results

3.1 Concomitant modulation of CO_2 and O_2 concentrations

A key component of our multiparametric hemodynamic imaging technique is the concomitant modulation of CO_2 and O_2 concentrations in the blood within the scan time of one exam. This is achieved with a CO_2 and O_2 breathing paradigm shown in Figure 1a,

using an MR-compatible gas-inhalation system depicted in Figure 1b. Note that, by "concomitant modulation", we are not suggesting that CO_2 and O_2 concentrations are altered synchronously with the same timing. Instead, as shown in Figure 1c, our breathing paradigm intends to modulate CO_2 and O_2 independently with different modulation frequencies. Across all participants studied, the cross-correlation coefficient (cc) between $EtCO_2$ and EtO_2 was found to be −0.12±0.09 (N=16). The slight anti-correlation between $EtCO_2$ and EtO_2 is due to the subject's hyperventilation during the hyperoxia period, which lowers $EtCO_2$. With the design of the concomitant paradigm, CO_2 and O_2 challenge data that would otherwise require separate exams can be collected in one scan. Consistent with our hypothesis, the BOLD MRI signal manifests modulatory effects from both gases but independently in timing (Figure 1d).

3.2 Estimation of hemodynamic images

Figures 3a and b depict hemodynamic maps of CVR and vCBV averaged across all healthy participants (N=7). CVR represents vasoactive response to a unit amount of blood CO_2 change (in %BOLD/mmHg CO_2), and reflects the extent of vascular reserve. The gray and white matter CVR values were 0.23±0.03 %/mmHg and 0.11±0.02 %/mmHg, respectively. vCBV is a marker of venous vascular space (%BOLD/mmHg O_2), and reflects baseline perfusion. The gray and white matter vCBV values were 0.0056±0.0006 %/mmHg and 0.0026±0.0004 %/mmHg, respectively. The gray matter has a greater CVR and vCBV compared to the white matter ($p<0.0001$). Note that, although CVR and vCBV maps are of similar image contrast in healthy participants, they reflect different types of physiological information. Their differential sensitivity becomes more apparent in patients when one parameter but not the other is compromised (see below).

We compared the CVR and vCBV maps obtained with concomitant gas modulation to those obtained with separate CO_2 and O_2 breathing paradigms. The maps acquired with the concomitant and separate CO_2/O_2 breathing were highly consistent. Quantitative analysis on regions of interest also showed a strong correlation ($r=0.96$ for CVR, and $r=0.91$ for vCBV) between the concomitant and separate breathing paradigms.

Figure 3c depicts the BAT map averaged across the participants (N=7). The gray matter manifests a shorter BAT compared to the white matter ($p<0.002$), as the cerebral vascular anatomy is such that the vessel needs to penetrate the gray matter before entering the white matter.

Figure 3d displays functional connectivity networks estimated from the concomitant gas-inhalation MRI data. Four representative networks, the default mode network (DMN), sensorimotor network, left fronto-parietal network, and right frontoparietal network, are shown, but other networks were also identified. Importantly, all parametric maps shown in Figure 3 were obtained from a single dataset of nine minutes.

3.3 Clinical evaluation of the technique in patients with Moyamoya syndrome

Nine patients with clinically-diagnosed Moyamoya syndrome underwent the MRI scan with concomitant CO_2 and O_2 breathing. Patient demographic and clinical information is shown in Table 1. All patients had radiographic appearance of a Moyamoya pattern of

neovascularization. Five patients had primary Moyamoya disease. All patients were able to complete the breathing task without complaint or adverse effects.

Figure 4 shows the CVR and vCBV maps of each patient, together with the averaged maps of the healthy controls. For reference, the patients' MRI angiograms are also shown, illustrating the specific arterial stenoses. Visual inspection suggested a diminished CVR in brain regions that correspond to the perfusion territory of the stenotic arteries. In contrast to deficits observed on the CVR images, venous CBV is slightly higher in diseased brain regions, possibly due to the large amount of collateral vessels compensatory to stenosis. Since Moyamoya syndrome is known to affect anterior cerebral artery (ACA) and middle cerebral artery (MCA) perfusion territories more than posterior cerebral artery (PCA) territories, we compared CVR between these territories. It was found that CVR in ACA/MCA regions was significantly lower than that in PCA (0.12±0.06 %/mmHg vs. 0.21±0.05 %/mmHg, p=0.0002).

Figure 5a shows BAT maps of individual patients. It can be seen that brain regions affected by stenosis tend to have longer BAT values. Compared to PCA territories, ACA/MCA regions have a significantly greater BAT (27.3±5.7s vs 20.7±1.9s, p=0.008). Time-to-peak (TTP) maps measured with conventional contrast-enhanced CT perfusion are displayed in Figure 5b. It can be seen that the two maps show excellent consistency, suggesting that BAT measured with gas-inhalation MRI can provide similar bolus timing information as perfusion CT.

Figure 6 shows functional connectivity maps of two representative networks computed using data of the concomitant CO_2 and O_2 breathing challenge. For comparison, results using conventional resting-state fMRI are also displayed. It can be seen that functional connectivity networks can be reliably determined from the gas-inhalation data and that the results are highly consistent with those using a conventional resting-state scan. To quantitatively evaluate the consistency between functional connectivity maps measured with the gas-inhalation data and the conventional resting-state data, we computed their spatial correlation. The correlation coefficient was 0.58±0.17 and 0.64±0.20 for the default mode network and primary visual network, respectively.

4. Discussion

In this work, we described a comprehensive framework integrating acquisition and analysis methods that can provide a non-invasive assessment of multiple hemodynamic parameters in the human brain. This method is rapid, reliable, and has the potential to be used in clinical studies of brain perfusion imaging.

Brain hemodynamic imaging provides critical information in a number of brain diseases. In stroke and cerebrovascular disease, blood supply and its reserve are important indicators of ischemia and can in turn guide treatment decisions (Zaca et al., 2011). In brain tumors, angiogenesis is an important marker of tumor aggressiveness and neovascularization often results in vessels that are poorly organized and lack vasodilatory capacity (Hsu et al., 2004;

Pillai and Zaca, 2012). In Alzheimer's disease, brain perfusion is thought to play a major role in the clearance of beta-amyloid (Sagare et al., 2012).

Current hemodynamic imaging techniques suffer from several limitations that the proposed approach can potentially overcome. Most notably, brain vascular health cannot be characterized by a single parameter. Instead, it is a complex system that requires multi-faceted examination in both baseline and challenged states. Current clinical practice requires several sessions or visits to obtain such complete information, which increases patient burden and cost of care. The proposed approach to complete these exams in a single MRI scan of less than 10 min represents an improvement in terms of clinical workflow. A second limitation of the current clinical hemodynamic imaging methods is that they all require the injection of an exogenous contrast agent (iodinated contrast materials for CT, Technetium-99m-labeled radiopharmaceuticals for SPECT, and gadolinium-based contrast agent, GBCA, for MRI). These agents increase exam costs, can cause allergic reactions, and are not approved for patients with low glomerular filtration rate (GFR). A recent study also reported that intravenous exposures to GBCA is associated with dose-dependent deposition in neuronal tissues even in patients with normal renal function (McDonald et al., 2015), suggesting greater risks than previously thought. Similarly, current vascular reactivity measurements are based on SPECT imaging, which requires the injection of radioactive tracers. This is not suitable for certain populations such as pediatric patients. Thus, the use of CO_2 and O_2 as a more biocompatible imaging agent is expected to benefit a broad range of patients, and is particularly useful for patients who cannot undergo currently available procedures. Moreover, this technique provides an excellent screening and monitoring tool as it can be repeated as many times as needed without concerns of radiation exposure or dosing limit of exogenous contrast agents.

The hemodynamic parameters measured with the proposed technique have distinctive but complementary values in brain diseases. CBV, an index of the amount of blood in the brain, has been shown to be an accurate marker for grading tumors (Law et al., 2004) and predicting their time to progression (Law et al., 2008). CVR indicates the ability of a blood vessel to dilate upon demand, and is a direct indicator of vascular reserve. CVR has an important value in chronic ischemic conditions such as atherosclerotic arterial steno-occlusive disease and Moyamoya disease (Donahue et al., 2013; Gupta et al., 2012; Mandell et al., 2008; Mikulis et al., 2005), and can guide clinical decision making between medical versus interventional treatments such as stenting or angioplasty (Pandya et al., 2015). The proposed method can potentially replace the current clinical method of SPECT with Diamox. BAT provides the kinetic property of cerebral blood supply. Such timing information has been used in acute stroke to determine the territory of ischemia penumbra (Wintermark et al., 2006), which can help select patients for use of intravascular tissue plasminogen activator (tPA). Functional connectivity MRI is now widely used in a variety of brain diseases for the assessment of brain function under pathological conditions. This information can be used to predict cognitive deficits in dementia (Greicius, 2008), tumors (Zhang et al., 2009), or cerebrovascular disorders (Lv et al., 2013). Therefore, the collection of all of the above information in a one-stop-shop can provide a thorough examination of the patient in a more efficient and cost-effective manner.

We have compared the results of the proposed technique by comparison with existing methods. CVR and vCBV maps obtained with the concomitant CO_2 and O_2 breathing paradigm were consistent with those obtained by separate CO_2-only or O_2-only paradigm. BAT maps using gas as a bolus are comparable to those obtained in CT perfusion. The BAT obtained from this method includes bolus arrival delay and vascular response time to the bolus (Thomas et al., 2014), but is more sensitive to the bolus arrival delay based on simulation findings. FC maps obtained in our technique were also similar to those obtained with conventional resting-state fMRI acquired with a separate scan. These results suggest good accuracy of our technique in measuring hemodynamic parameters. However, a limitation of the current study is the lack of comparison of our CVR mapping technique to gold -standard. SPECT imaging is the current gold standard for CVR measurement. However, in our institution, patients receive either CT or SPECT (but not both) for perfusion imaging. All patients included in this study have received perfusion CT, which provided a validation measure for BAT as reported above, but they did not receive SPECT imaging. We have an ongoing study to recruit patients who undergo SPECT Diamox imaging, which will provide a validation of CVR results. These findings will be reported in a future study.

For the data analysis in our method, we have compared the smoothness of 8mm, 6mm and 4mm. CVR and vCBV maps with good quality can be obtained with all three smoothness (Supplemental Figure S2 for healthy subjects and S3 for Moyamoya patients). We found that for Moyamoya patients, CVR maps with 8mm smoothness showed better differentiation between the CVR-deficit regions and normal regions. For future studies, different smoothness can be chosen based on the size of brain abnormalities.

A limitation of this technique is that it cannot be used in unconscious patients because of the need of a breathing task. In that case, natural variation in blood CO_2 content could potentially be used to evaluate CVR, BAT, and FC, but not vCBV. In this study, all of the healthy volunteers and Moyamoya patients were able to finish the MRI scan with the breathing task, suggesting that this technique is feasible and practical in conscious patients. Additionally, the use of of nose clip and mouthpiece may not be suitable for young children, patients with asthma or other chronic breathing impairment, and patients that requires constant O_2 inhaler. But the use of nose clip and mouthpiece requires smaller amount of space inside head coil comparing to the use of face masks. This is a potential advantage as head coils are increasingly made smaller for better coil sensitivity. Moreover, the concomitant CO_2 and O_2 breathing paradigm proposed in this study is independent of our gas delivery methods. It can be applied with other delivery methods and systems as well. We also observed that quantitative values of CVR and vCBV obtained from the concomitant CO_2 and O_2 breathing challenge was slightly higher than that obtained from separate breathing challenges. This may be because, in our analysis, we linearized the BOLD biophysical equation (Gauthier and Hoge, 2013; Hoge et al., 1999) in order to conduct regression analysis of both CO_2 and O_2 time courses. It is possible that this may produce some small biases (Hare et al., 2013). For example, the vCBV we measured could be a weighted average of normocapnic vCBV and hypercapnic vCBV. Additionally, potential effects of gas inhalation on cerebral metabolism could also cause a signal difference in BOLD (Xu et al., 2012; Xu et al., 2011). Another limitation is that in CVR mapping, the BOLD signal is not a direct measure of CBF change in the brain. However, current dual-

echo ASL/BOLD sequence is slow in acquisition and its sensitivity in detecting dynamic CBF change requires some improvements. Therefore, we used BOLD sequence in our method due to its faster sampling rate and superior sensitivity (similar to the situation in the fMRI field). When ASL sensitivity is further enhanced, for example by high field imaging or better labeling schemes, dual-echo ASL/BOLD sequence will provide an approach for CVR mapping with direct physiological units (Bulte et al., 2012; Gauthier and Hoge, 2012; Wise et al., 2013).

5. Conclusions

This study demonstrates the feasibility of a novel imaging method to assess cerebrovascular hemodynamics using gas-inhalation MRI. With the proposed approach, a single MRI scan of less than 10 minutes allows the measurement of multiple (including baseline and reserve) vascular properties without the need for radiation exposure or administration of exogenous contrast agents. This technique can significantly reduce patient burden and the cost of care in clinical perfusion imaging and also provides an important alternative to existing imaging methods for patients who are allergic to contrast agent.

Supplementary Material

Refer to Web version on PubMed Central for supplementary material.

Acknowledgements

This study was supported in part by NIH R01 AG042753 (to H.L.), NIH R01 MH084021 (to H.L.), NIH R21 NS095342 (to H.L.), and NIH R21 NS085634 (to P.L.).

Reference

Beckmann CF, DeLuca M, Devlin JT, Smith SM. Investigations into resting-state connectivity using independent component analysis. Philos Trans R Soc Lond B Biol Sci. 2005; 360:1001–1013. [PubMed: 16087444]

Blockley NP, Griffeth VE, Germuska MA, Bulte DP, Buxton RB. An analysis of the use of hyperoxia for measuring venous cerebral blood volume: comparison of the existing method with a new analysis approach. Neuroimage. 2013; 72:33–40. [PubMed: 23370053]

Brian JE Jr. Carbon dioxide and the cerebral circulation. Anesthesiology. 1998; 88:1365–1386. [PubMed: 9605698]

Bright MG, Donahue MJ, Duyn JH, Jezzard P, Bulte DP. The effect of basal vasodilation on hypercapnic and hypocapnic reactivity measured using magnetic resonance imaging. Journal of Cerebral Blood Flow & Metabolism. 2011; 31:426–438. [PubMed: 20959855]

Brueckl C, Kaestle S, Kerem A, Habazettl H, Krombach F, Kuppe H, Kuebler WM. Hyperoxia-induced reactive oxygen species formation in pulmonary capillary endothelial cells in situ. Am J Respir Cell Mol Biol. 2006; 34:453–463. [PubMed: 16357365]

Bulte D, Chiarelli P, Wise R, Jezzard P. Measurement of cerebral blood volume in humans using hyperoxic MRI contrast. Journal of Magnetic Resonance Imaging. 2007; 26:894–899. [PubMed: 17896390]

Bulte DP, Kelly M, Germuska M, Xie J, Chappell MA, Okell TW, Bright MG, Jezzard P. Quantitative measurement of cerebral physiology using respiratory-calibrated MRI. Neuroimage. 2012; 60:582–591. [PubMed: 22209811]

Burt RW, Witt RM, Cikrit DF, Reddy RV. Carotid artery disease: evaluation with acetazolamide-enhanced Tc-99m HMPAO SPECT. Radiology. 1992; 182:461–466. [PubMed: 1732965]

Carter AR, Shulman GL, Corbetta M. Why use a connectivity-based approach to study stroke and recovery of function? Neuroimage. 2012; 62:2271–2280. [PubMed: 22414990]

Chan ST, Evans KC, Rosen BR, Song TY, Kwong KK. A case study of magnetic resonance imaging of cerebrovascular reactivity: a powerful imaging marker for mild traumatic brain injury. Brain Inj. 2015; 29:403–407. [PubMed: 25384127]

Chollet F, Celsis P, Clanet M, Guiraud-Chaumeil B, Rascol A, Marc-Vergnes JP. SPECT study of cerebral blood flow reactivity after acetazolamide in patients with transient ischemic attacks. Stroke. 1989; 20:458–464. [PubMed: 2784599]

Detre JA, Leigh JS, Williams DS, Koretsky AP. Perfusion imaging. Magn Reson Med. 1992; 23:37–45. [PubMed: 1734182]

Donahue MJ, Ayad M, Moore R, van Osch M, Singer R, Clemmons P, Strother M. Relationships between hypercarbic reactivity, cerebral blood flow, and arterial circulation times in patients with moyamoya disease. J Magn Reson Imaging. 2013 In-press. doi: 10.1002/jmri.24070.

Donahue MJ, Dethrage LM, Faraco CC, Jordan LC, Clemmons P, Singer R, Mocco J, Shyr Y, Desai A, O'Duffy A, Riebau D, Hermann L, Connors J, Kirshner H, Strother MK. Routine clinical evaluation of cerebrovascular reserve capacity using carbogen in patients with intracranial stenosis. Stroke. 2014; 45:2335–2341. [PubMed: 24938845]

Gauthier CJ, Hoge RD. Magnetic resonance imaging of resting OEF and CMRO(2) using a generalized calibration model for hypercapnia and hyperoxia. Neuroimage. 2012; 60:1212–1225. [PubMed: 22227047]

Gauthier CJ, Hoge RD. A generalized procedure for calibrated MRI incorporating hyperoxia and hypercapnia. Hum Brain Mapp. 2013; 34:1053–1069. [PubMed: 23015481]

Geranmayeh F, Wise RJ, Leech R, Murphy K. Measuring vascular reactivity with breath-holds after stroke: a method to aid interpretation of group-level BOLD signal changes in longitudinal fMRI studies. Hum Brain Mapp. 2015; 36:1755–1771. [PubMed: 25727648]

Greenberg SM. Small vessels, big problems. N Engl J Med. 2006; 354:1451–1453. [PubMed: 16598043]

Greicius M. Resting-state functional connectivity in neuropsychiatric disorders. Curr Opin Neurol. 2008; 21:424–430. [PubMed: 18607202]

Gupta A, Chazen JL, Hartman M, Delgado D, Anumula N, Shao H, Mazumdar M, Segal AZ, Kamel H, Leifer D, Sanelli PC. Cerebrovascular reserve and stroke risk in patients with carotid stenosis or occlusion: a systematic review and meta-analysis. Stroke. 2012; 43:2884–2891. [PubMed: 23091119]

Han JS, Mandell DM, Poublanc J, Mardimae A, Slessarev M, Jaigobin C, Fisher JA, Mikulis DJ. BOLD-MRI cerebrovascular reactivity findings in cocaine-induced cerebral vasculitis. Nat Clin Pract Neurol. 2008; 4:628–632. [PubMed: 18839005]

Hare HV, Germuska M, Kelly ME, Bulte DP. Comparison of CO2 in air versus carbogen for the measurement of cerebrovascular reactivity with magnetic resonance imaging. J Cereb Blood Flow Metab. 2013; 33:1799–1805. [PubMed: 23921896]

Hirano T, Minematsu K, Hasegawa Y, Tanaka Y, Hayashida K, Yamaguchi T. Acetazolamide reactivity on 123I-IMP single photon emission computed tomography in patients with major cerebral artery occlusive disease: correlation with positron emission tomography parameters. J Cereb Blood Flow Metab. 1994; 14:763–770. [PubMed: 8063872]

Hoge RD, Atkinson J, Gill B, Crelier GR, Marrett S, Pike GB. Investigation of BOLD signal dependence on cerebral blood flow and oxygen consumption: the deoxyhemoglobin dilution model. Magn Reson Med. 1999; 42:849–863. [PubMed: 10542343]

Hsu YY, Chang CN, Jung SM, Lim KE, Huang JC, Fang SY, Liu HL. Blood oxygenation level-dependent MRI of cerebral gliomas during breath holding. J Magn Reson Imaging. 2004; 19:160–167. [PubMed: 14745748]

Law M, Yang S, Babb JS, Knopp EA, Golfinos JG, Zagzag D, Johnson G. Comparison of cerebral blood volume and vascular permeability from dynamic susceptibility contrast-enhanced perfusion MR imaging with glioma grade. AJNR Am J Neuroradiol. 2004; 25:746–755. [PubMed: 15140713]

Law M, Young RJ, Babb JS, Peccerelli N, Chheang S, Gruber ML, Miller DC, Golfinos JG, Zagzag D, Johnson G. Gliomas: predicting time to progression or survival with cerebral blood volume measurements at dynamic susceptibility-weighted contrast-enhanced perfusion MR imaging. Radiology. 2008; 247:490–498. [PubMed: 18349315]

Lerman C, Gu H, Loughead J, Ruparel K, Yang Y, Stein EA. Large-scale brain network coupling predicts acute nicotine abstinence effects on craving and cognitive function. JAMA Psychiatry. 2014; 71:523–530. [PubMed: 24622915]

Lu H, Liu P, Yezhuvath U, Cheng Y, Marshall O, Ge Y. MRI mapping of cerebrovascular reactivity via gas inhalation challenges. J Vis Exp. 2014

Lu H, Pollack E, Young R, Babb JS, Johnson G, Zagzag D, Carson R, Jensen JH, Helpern JA, Law M. Predicting grade of cerebral glioma using vascular-space occupancy MR imaging. AJNR Am J Neuroradiol. 2008; 29:373–378. [PubMed: 17974612]

Lu H, Xu F, Rodrigue KM, Kennedy KM, Cheng Y, Flicker B, Hebrank AC, Uh J, Park DC. Alterations in cerebral metabolic rate and blood supply across the adult lifespan. Cereb Cortex. 2011; 21:1426–1434. [PubMed: 21051551]

Lv Y, Margulies DS, Cameron Craddock R, Long X, Winter B, Gierhake D, Endres M, Villringer K, Fiebach J, Villringer A. Identifying the perfusion deficit in acute stroke with resting-state functional magnetic resonance imaging. Ann Neurol. 2013; 73:136–140. [PubMed: 23378326]

Mandell DM, Han JS, Poublanc J, Crawley AP, Stainsby JA, Fisher JA, Mikulis DJ. Mapping cerebrovascular reactivity using blood oxygen level-dependent MRI in Patients with arterial steno-occlusive disease: comparison with arterial spin labeling MRI. Stroke. 2008; 39:2021–2028. [PubMed: 18451352]

Marckmann P, Skov L, Rossen K, Dupont A, Damholt MB, Heaf JG, Thomsen HS. Nephrogenic systemic fibrosis: suspected causative role of gadodiamide used for contrast-enhanced magnetic resonance imaging. J Am Soc Nephrol. 2006; 17:2359–2362. [PubMed: 16885403]

Mark CI, Pike GB. Indication of BOLD-specific venous flow-volume changes from precisely controlled hyperoxic vs. hypercapnic calibration. J Cereb Blood Flow Metab. 2012; 32:709–719. [PubMed: 22167238]

Marshall O, Lu H, Brisset JC, Xu F, Liu P, Herbert J, Grossman RI, Ge Y. Impaired cerebrovascular reactivity in multiple sclerosis. JAMA Neurol. 2014; 71:1275–1281. [PubMed: 25133874]

McDonald RJ, McDonald JS, Kallmes DF, Jentoft ME, Murray DL, Thielen KR, Williamson EE, Eckel LJ. Intracranial Gadolinium Deposition after Contrast-enhanced MR Imaging. Radiology. 2015; 275:772–782. [PubMed: 25742194]

Mikulis DJ, Krolczyk G, Desal H, Logan W, Deveber G, Dirks P, Tymianski M, Crawley A, Vesely A, Kassner A, Preiss D, Somogyi R, Fisher JA. Preoperative and postoperative mapping of cerebrovascular reactivity in moyamoya disease by using blood oxygen level-dependent magnetic resonance imaging. J Neurosurg. 2005; 103:347–355. [PubMed: 16175867]

Ogasawara K, Ito H, Sasoh M, Okuguchi T, Kobayashi M, Yukawa H, Terasaki K, Ogawa A. Quantitative measurement of regional cerebrovascular reactivity to acetazolamide using 123I-N-isopropyl-p-iodoamphetamine autoradiography with SPECT: validation study using H2 15O with PET. J Nucl Med. 2003; 44:520–525. [PubMed: 12679394]

Ostergaard L, Weisskoff RM, Chesler DA, Gyldensted C, Rosen BR. High resolution measurement of cerebral blood flow using intravascular tracer bolus passages. Part I: Mathematical approach and statistical analysis. Magn Reson Med. 1996; 36:715–725. [PubMed: 8916022]

Pandya A, Gupta A, Kamel H, Navi BB, Sanelli PC, Schackman BR. Carotid artery stenosis: cost-effectiveness of assessment of cerebrovascular reserve to guide treatment of asymptomatic patients. Radiology. 2015; 274:455–463. [PubMed: 25225841]

Park CH, Chang WH, Ohn SH, Kim ST, Bang OY, Pascual-Leone A, Kim YH. Longitudinal changes of resting-state functional connectivity during motor recovery after stroke. Stroke. 2011; 42:1357–1362. [PubMed: 21441147]

Pillai JJ, Zaca D. Clinical utility of cerebrovascular reactivity mapping in patients with low grade gliomas. World J Clin Oncol. 2011; 2:397–403. [PubMed: 22171282]

Pillai JJ, Zaca D. Comparison of BOLD cerebrovascular reactivity mapping and DSC MR perfusion imaging for prediction of neurovascular uncoupling potential in brain tumors. Technol Cancer Res Treat. 2012; 11:361–374. [PubMed: 22376130]

Ravi H, Thomas BP, Peng SL, Liu H, Lu H. On the optimization of imaging protocol for the mapping of cerebrovascular reactivity. J Magn Reson Imaging. 2015

Reichenbach JR, Rother J, Jonetz-Mentzel L, Herzau M, Fiala A, Weiller C, Kaiser WA. Acute stroke evaluated by time-to-peak mapping during initial and early follow-up perfusion CT studies. AJNR Am J Neuroradiol. 1999; 20:1842–1850. [PubMed: 10588107]

Sagare AP, Bell RD, Zlokovic BV. Neurovascular dysfunction and faulty amyloid beta-peptide clearance in Alzheimer disease. Cold Spring Harb Perspect Med 2. 2012

Sheng M, Lu H, Liu P, Thomas BP, McAdams CJ. Cerebral perfusion differences in women currently with and recovered from anorexia nervosa. Psychiatry Res. 2015; 232:175–183. [PubMed: 25795596]

Spano VR, Mandell DM, Poublanc J, Sam K, Battisti-Charbonney A, Pucci O, Han JS, Crawley AP, Fisher JA, Mikulis DJ. CO2 blood oxygen level-dependent MR mapping of cerebrovascular reserve in a clinical population: safety, tolerability, and technical feasibility. Radiology. 2013; 266:592–598. [PubMed: 23204541]

Thomas BP, Liu P, Park DC, van Osch MJ, Lu H. Cerebrovascular reactivity in the brain white matter: magnitude, temporal characteristics, and age effects. J Cereb Blood Flow Metab. 2014; 34:242–247. [PubMed: 24192640]

Wintermark M, Flanders AE, Velthuis B, Meuli R, van Leeuwen M, Goldsher D, Pineda C, Serena J, van der Schaaf I, Waaijer A, Anderson J, Nesbit G, Gabriely I, Medina V, Quiles A, Pohlman S, Quist M, Schnyder P, Bogousslavsky J, Dillon WP, Pedraza S. Perfusion-CT assessment of infarct core and penumbra: receiver operating characteristic curve analysis in 130 patients suspected of acute hemispheric stroke. Stroke. 2006; 37:979–985. [PubMed: 16514093]

Wintermark M, Maeder P, Verdun FR, Thiran JP, Valley JF, Schnyder P, Meuli R. Using 80 kVp versus 120 kVp in perfusion CT measurement of regional cerebral blood flow. AJNR Am J Neuroradiol. 2000; 21:1881–1884. [PubMed: 11110541]

Wise RG, Harris AD, Stone AJ, Murphy K. Measurement of OEF and absolute CMRO2: MRI-based methods using interleaved and combined hypercapnia and hyperoxia. Neuroimage. 2013; 83:135–147. [PubMed: 23769703]

Xu F, Liu P, Pascual JM, Xiao G, Lu H. Effect of hypoxia and hyperoxia on cerebral blood flow, blood oxygenation, and oxidative metabolism. J Cereb Blood Flow Metab. 2012; 32:1909–1918. [PubMed: 22739621]

Xu F, Uh J, Brier MR, Hart J Jr. Yezhuvath US, Gu H, Yang Y, Lu H. The influence of carbon dioxide on brain activity and metabolism in conscious humans. J Cereb Blood Flow Metab. 2011; 31:58–67. [PubMed: 20842164]

Yezhuvath US, Lewis-Amezcua K, Varghese R, Xiao G, Lu H. On the assessment of cerebrovascular reactivity using hypercapnia BOLD MRI. NMR Biomed. 2009; 22:779–786. [PubMed: 19388006]

Yezhuvath US, Uh J, Cheng Y, Martin-Cook K, Weiner M, Diaz-Arrastia R, van Osch M, Lu H. Forebrain-dominant deficit in cerebrovascular reactivity in Alzheimer's disease. Neurobiol Aging. 2012; 33:75–82. [PubMed: 20359779]

Zaca D, Hua J, Pillai JJ. Cerebrovascular reactivity mapping for brain tumor presurgical planning. World J Clin Oncol. 2011; 2:289–298. [PubMed: 21773079]

Zhang D, Johnston JM, Fox MD, Leuthardt EC, Grubb RL, Chicoine MR, Smyth MD, Snyder AZ, Raichle ME, Shimony JS. Preoperative sensorimotor mapping in brain tumor patients using spontaneous fluctuations in neuronal activity imaged with functional magnetic resonance imaging: initial experience. Neurosurgery. 2009; 65:226–236. [PubMed: 19934999]

Highlights

* A novel MRI method was proposed for multiparametric hemodynamic imaging.

* This method concomitantly measures CBV, CVR, BAT, and functional connectivity.

* The method combines new gas-inhalation paradigms with advanced analysis algorithm.

* Its utility was demonstrated in healthy subjects and in Moyamoya syndrome.

* This technique can significantly reduce patient burden and cost of clinical care.

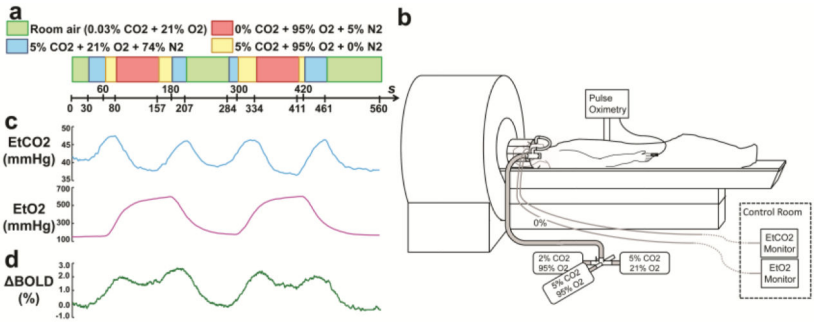

Figure 1.

Illustration of the concomitant CO_2 and O_2 modulation. (a) Paradigm of the gas inhalation. (b) Demonstration of the MRI-compatible gas delivery system. (c) Averaged $EtCO_2$, Et O_2 and ΔBOLD signal time courses from the healthy subjects.

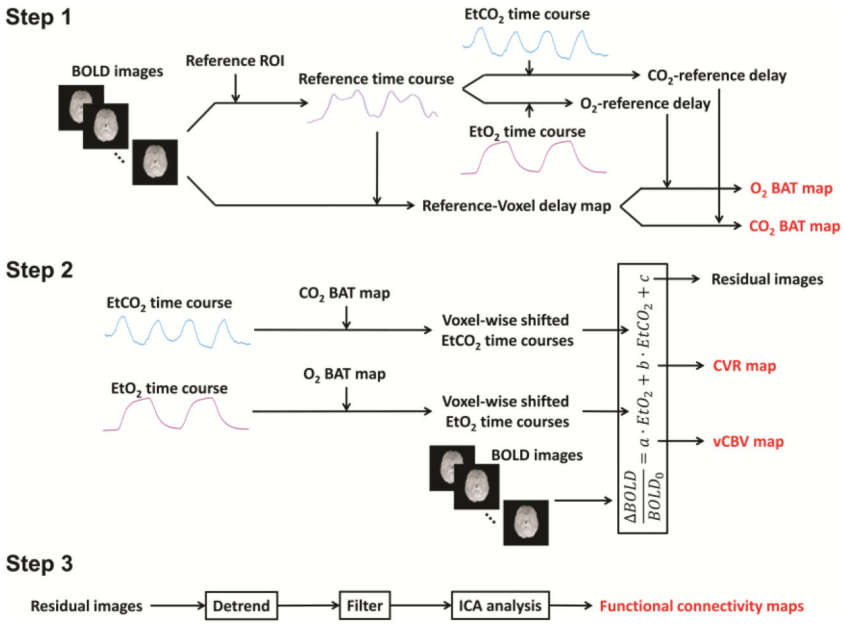

Figure 2.

Illustration of analysis steps in the multiparametric imaging method to obtain bolus arrival time (BAT), cerebrovascular reactivity (CVR), venous cerebral blood volume (vCBV) and functional connectivity maps.

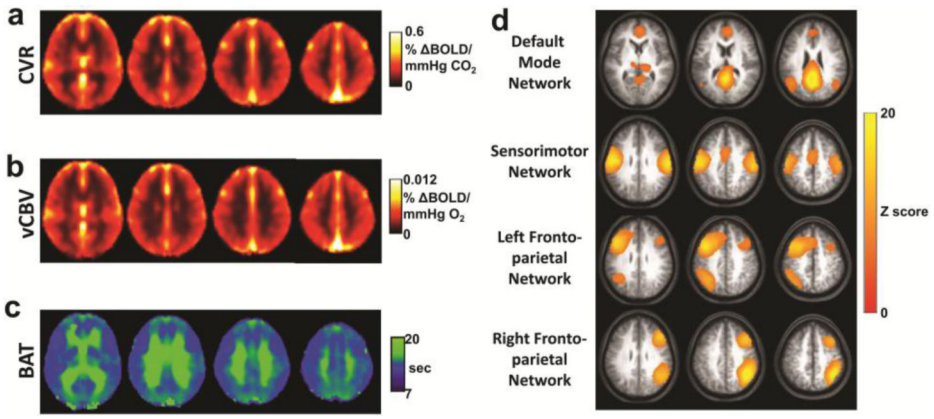

Figure 3.

Group results from the healthy subjects (N=7). (a) Averaged CVR map. (b) Averaged vCBV map. (c) Averaged CO_2-BAT map. (d) Examples of the functional connectivity networks obtained from group ICA analysis.

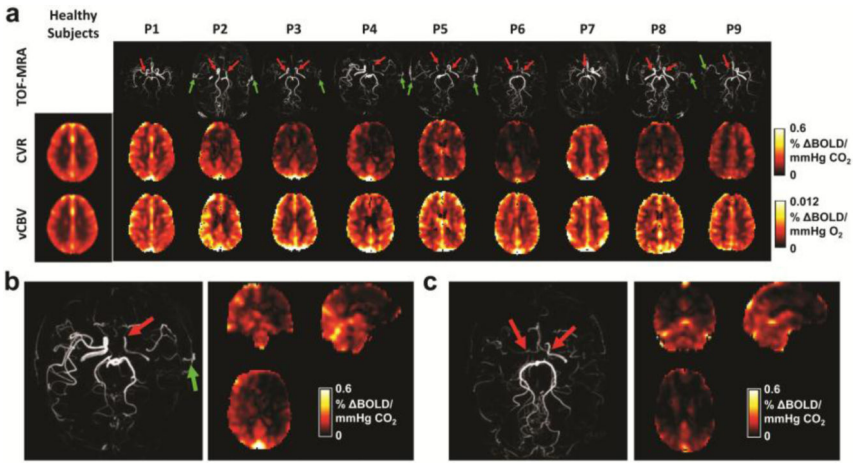

Figure 4.

Results from the Moyamoya patients. (a) CVR and vCBV maps of all patients (N=9). The TOF-MRA shows the diseased vessels (red arrows) and revascularizations (green arrows). (b) TOF MRA and the CVR map of patient P4 who has left side stenosis. (c) TOF MRA and the CVR map of patient P6 who has bilateral stenosis.

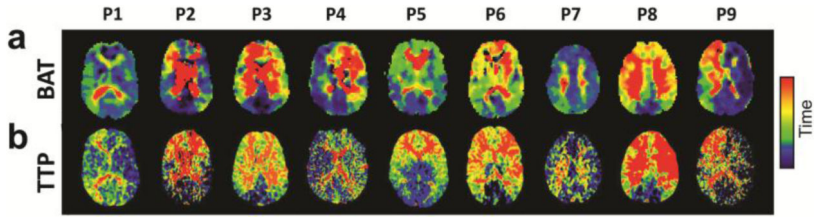

Figure 5.
Qualitative comparison of the BAT maps obtained from the MRI scan and the TTP maps obtained from the CTP scan.

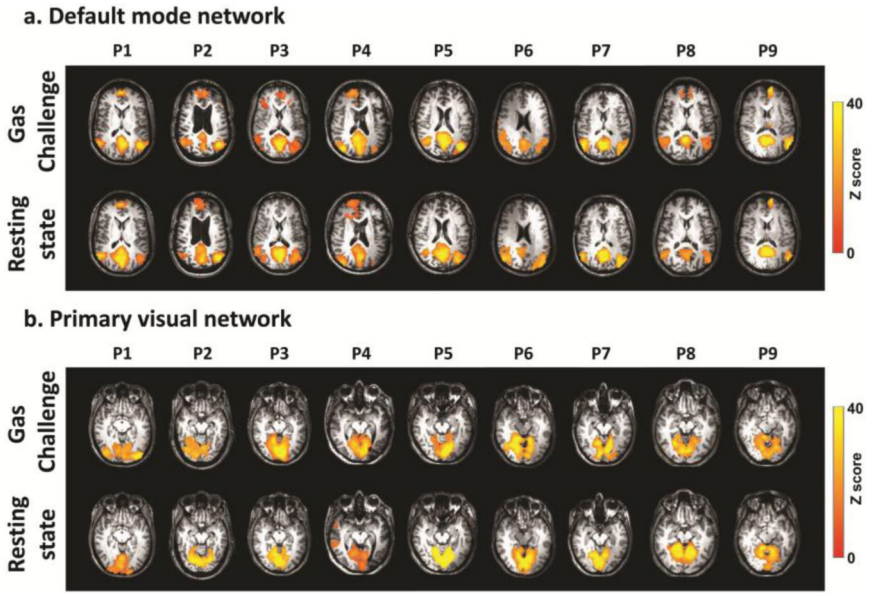

Figure 6.

Examples of the functional connectivity networks obtained from individual ICA analysis in Moyamoya patients (N=9). (a) Maps of the default mode networks. (b) Maps of the primary visual networks. Top rows show the results from conventional resting-state fMRI scan without gas inhalation. Bottom rows show the results from the fMRI scan with concomitant CO_2 and O_2 challenge.

Table 1

Demographic information of the Moyamoya patients.

Subject	Age	Gender	Diagnosis	Treatment
P1	50	F	Right supraclinoid stenosis	Angioplasty
P2	49	F	Bilateral supraclinoid stenosis	Bilateral bypasses
P3	30	F	Bilateral supraclinoid occlusions	Left bypass; right untreated
P4	48	F	Left supraclinoid ICA occlusion	Bypass
P5	31	M	Bilateral supraclinoid occlusions	Bilateral bypass
P6	60	F	Bilateral cavernous/supraclinoid disease	Untreated
P7	45	F	Right supraclinoid disease	Untreated
P8	35	M	Bilateral MCA occlusions	Left bypass
P9	38	F	Right ICA occlusion	Right bypass